IEEE Access
Multidisciplinary ⁝ Rapid Review ⁝ Open Access Journal

Received 30 September 2025, accepted 17 October 2025, date of publication 23 October 2025, date of current version 31 October 2025.

Digital Object Identifier 10.1109/ACCESS.2025.3624458

RESEARCH ARTICLE

Designs of Automotive High-Gain TM_{05}-Mode Patch Array Antennas

TING-WEI KUO[1], YU-LIANG ZHU CHEN[1], ERIC S. LI[2], HUAYAN JIN[3], (Member, IEEE), DONGXU CHEN[4], NORUN FARIHAH ABDUL MALEK[5], (Senior Member, IEEE), AND KUO-SHENG CHIN[1], (Senior Member, IEEE)

[1]Department of Electronic Engineering, Chang Gung University, Taoyuan 33302, Taiwan
[2]Department of Electronic Engineering, National Taipei University of Technology, Taipei 10608, Taiwan
[3]Key Laboratory of RF Circuits and Systems of Ministry of Education, Xiasha High Education Park, Hangzhou Dianzi University, Hangzhou 310018, China
[4]Computer and Information College, Hohai University, Nanjing, Jiangsu 210098, China
[5]Department of Electrical and Computer Engineering, International Islamic University Malaysia, Kuala Lumpur 53100, Malaysia

Corresponding author: Kuo-Sheng Chin (kschin@mail.cgu.edu.tw)

This work was supported in part by the National Science and Technology Council, Taiwan, under Grant NSTC 114-2221-E-182-037.

ABSTRACT This work presents the design and implementation of three TM_{05}-mode patch array antennas for automotive radar applications, featuring high gain, low sidelobe level (SLL), and enhanced bandwidth. To improve radiation performance, patches in TM_{05} mode are employed with surface-etched slots to suppress reverse currents, thereby increasing gain and reducing SLLs. Antenna I is a 79-GHz 2 × 8 TM_{05}-mode patch array antenna fed by a substrate-integrated waveguide (SIW) network with differential excitation to minimize cross-polarization. An SIW-based excitation design highlighting Taylor distribution is applied to further suppress sidelobes. Measured results show a −10 dB impedance bandwidth of 77.92−79.15 GHz (1.6%), a peak gain of 18.2 dBi, and a SLL of −19.1 dB in H-plane. The cross-polarization level is reduced to nearly 30 dB lower than the co-polarization level. Antenna II is a 77-GHz staggered series-fed six-element TM_{05}-mode patch array designed for compact integration. An in-phase excitation scheme with an array spacing of $3\lambda_g/2$ is proposed. This antenna achieves a measured bandwidth of 73.76–78.44 GHz (6.1%) and a high gain of 17.5 dBi with only six elements. Antenna III further introduces parasitic strips alongside each patch from Antenna II to generate additional resonances and to enhance bandwidth. Measured results exhibit a bandwidth of 72.64–80.75 GHz (10.57%) and a peak gain of 17.8 dBi, representing an increase of 4.47% in bandwidth compared to Antenna II. In summary, Antenna I achieves high gain, low SLL, and low cross-polarization with higher complexity, while Antennas II/III simplify design yet deliver high gain and wide bandwidth, offering promising solutions for automotive radars.

INDEX TERMS Automotive antenna, bandwidth enhancement, differential feeding, high-gain antenna, higher-order mode patch, sidelobe level suppression, staggered series feeding, TM_{05}-mode patch antenna.

I. INTRODUCTION

Automotive radars have become a fundamental unit in advanced driver-assistance systems (ADAS) and autonomous driving technologies. Depending on their detection range and functions, automotive radars are categorized into long-range radars (LRRs), medium-range radars (MRRs), and short-range radars (SRRs). LRR typically operates at 76−77 GHz, while MRR and SRR function at a wider band of 77−81 GHz. To support full-band operation, antennas must exhibit high gain and low sidelobe levels (SLLs) across 76−81 GHz (6.4%) to achieve great detection and to meet desired resolution.

Automotive radar antennas reported in recent literatures generally can be categorized into four groups: (1) microstrip planar patch arrays, (2) slot and grid arrays based on substrate-integrated waveguide (SIW), (3) leaky-wave antennas (LWAs), and (4) lens-based antennas and phased/MIMO

The associate editor coordinating the review of this manuscript and approving it for publication was Kai Lu.

arrays [1−21]. Typical examples of microstrip patch array designs include a 6×10 array with a peak gain of 20 dBi and SLLs of –15 dB in E-plane and –12 dB in H-plane [1]. An 8×18 null-filling proximity-coupled patch array optimized via genetic algorithms demonstrated a gain of 21.35 dBi and an H-plane SLL of –20.17 dB, albeit a more complex and bulky feeding network [2]. A 6×16 SIW-fed slot array offered a gain of 21.7 dBi and an H-plane SLL of –18 dB [3], while a dual-sided transmitting array with array elements arranged in a concentric ring reached a gain of 18.5 dBi at 76.5 GHz [4]. In [5], a patch array with a dual coupled feeding scheme allowed a stable gain of 11.5 dBi across the full band of 76–81 GHz. A traveling-wave series-fed patch array with a gain of 13.8 dBi was reported in [6], where SLL suppression was carried out by adjusting the radiated power from each element. Polarization diversity was addressed in [7], where dual-polarized operation was realized using a combination of vertically polarized series-fed patches and a horizontally polarized slotted leaky-wave structure. A split-ring resonator array with a series-coupled feed achieved a gain of 12.1 dBi and an H-plane SLL of –20 dB [8]. A multilayer cylindrical Luneburg lens composed of AirexR82 was proposed in [9], offering ±85° beam scanning in the azimuth plane. In [10], an end-fire antenna incorporating an I-shaped director enhanced gain performance.

Stacked patch configurations were utilized in [11] to realize an 8×6 array with a bandwidth of 5.2%, at the cost of increased layer complexity. A cavity-backed 6×10 patch array with an SIW feed extended bandwidth to 8.7% [12], and a differential-fed cavity-backed structure produced a bandwidth of 6.9% and a gain of 14.4 dBi [13]. Low-temperature co-fired ceramic (LTCC) technology was adopted in [14] for an 8×8 slot array using a microstrip-to-ridge gap waveguide transition, resulting in a bandwidth of 6% and a gain of 18.3 dBi. A dual-circularly polarized slot array based on ridge gap waveguide (RGW) provided a bandwidth of 10.9% [15], while an 8×8 cavity-backed slot array employing bowtie-shaped coupling slots supplied a bandwidth of 10% as well as a gain of 26.4 dBi [16]. Further innovations include a loop-based planar grid array with multiple resonant cells for gain-bandwidth enhancement [17], and a comb-line array that offered a compact size and stable gain bandwidth [18]. A periodic asymmetric trapezoidal perturbation microstrip array was presented in [19], utilizing staggered trapezoidal stubs to generate a trapezoidal cascade electric field for a bandwidth of 13%. To mitigate beam squint in series-fed patch arrays, an amplitude-phase adjustment method was introduced in [20]. Wide detection coverage was achieved in [21] through the design of sector-beam transmitting antennas based on phase-shifted series-fed patch arrays.

More recently, high-order mode patch antennas have been proposed, which have large gains and can reduce the number of elements and the complexity of feeding network in large-scale arrays [22], [23], [24], [25], [26], [27], [28]. In [22], a TM_{12}-mode patch was presented with etched slots to suppress reverse currents. A shorted patch with slots can simultaneously excite the TM_{30} and TM_{10} modes, and achieved a bandwidth of 18% by adjusting the dual-mode resonance [23]. Metal vias were selected to reduce SLL and to enhance gain. TM_{03}- and TM_{05}-mode patch designs [24], [25], [26] employed slot etching for surface current tuning to suppress undesired radiation. An anti-phase TM_{30}-mode patch with two unequal transverse slots demonstrated improved bandwidth and reduced cross-polarization [27], while modified TM_{30}- and TM_{50}-mode patches decreased out-of-phase current effects, yielding high directivity [28]. However, most of these high-order-mode patches operate below the frequency range of automotive radars, thus require further investigation for that application.

In view of the stringent requirements of automotive radars, three TM_{05}-mode patch array antennas are developed in this work to respectively achieve the goal of high gain, low SLL, and bandwidth enhancement within the band of 76–81 GHz. This paper is organized as follows: Section II presents the design for Antenna I, a 79-GHz 2×8 patch array with parallel differential feeding and slot loading, achieving high gain and low SLL. Section III introduces the design for Antenna II, a compact 6-element array using a staggered series feed to simplify design and size and achieve high gain at 77 GHz, followed by a description on Antenna III. The antenna integrates parasitic strips into Antenna II to generate additional resonant modes, thereby extending the bandwidth. At last, the paper is concluded in Section IV.

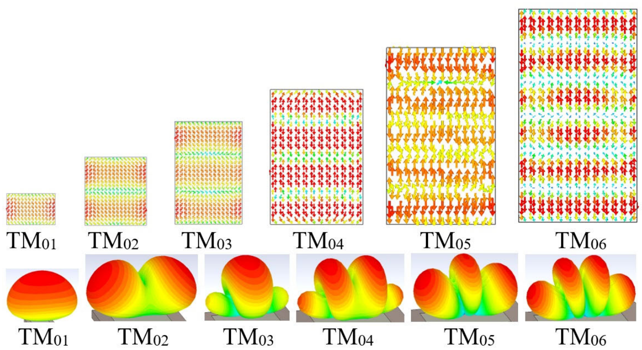

FIGURE 1. Surface current distributions and radiation patterns of the TM_{01} – TM_{06}-mode patches operating at 79 GHz.

II. 79-GHz DIFFERENTIAL-FED 2 × 8 TM_{05}-MODE PATCH ARRAY ANTENNA

A. ANALYSIS OF TM_{05}-MODE PATCH ANTENNA

A rectangular patch antenna exhibits a transverse magnetic field and an electric field along the z-direction. Based on a cavity model, the patch is allowed to operate in a TM_{mn} mode with the modal indices of m and n. The corresponding electric field and resonant frequency can be expressed as:

$$E_Z = E_0 \cos\frac{m\pi X}{W}\cos\frac{n\pi Y}{L} \tag{1a}$$

$$f_{mn} = \frac{c}{2\pi\sqrt{\varepsilon_r}}\sqrt{\left(\frac{m\pi}{W}\right)^2 + \left(\frac{n\pi}{L}\right)^2} \tag{1b}$$

where W and L are the width and length of the patch [29]. The condition of $m = 0$ is often applied to single polarization and simple structures. Fig. 1 shows the surface current distributions and radiation patterns of the first six modes of a rectangular patch, from TM_{01} to TM_{06}, at 79 GHz. Since the resonant currents reverse their directions for every $\lambda_g/2$ with λ_g being the guided wavelength, the even-mode currents of $TM_{0(2n)}(n = 1, 2\ldots)$ produce radiation nulls in the broadside direction, and therefore provide little contribution to its gain. The odd modes $TM_{0(2n+1)}$ $(n = 0, 1, 2\ldots)$, however, present $n + 1$ forward currents and n reverse currents. The reverse currents cause high SLLs. The patch in higher-order mode usually accompanies higher gain because of larger electric size, but it is also more difficult to control the reverse currents. Therefore, a TM_{05}-mode patch is a compromised choice for this work.

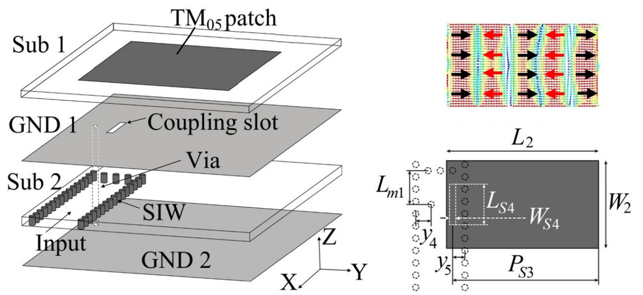

FIGURE 2. Configuration of the 79-GHz TM_{05}-mode patch. Each substrate is RO4003C, with $\varepsilon_r = 3.55$, $\tan\delta = 0.0027$, and a thickness of 0.305 mm. Dimensions: $L_2 = 4.95$, $W_2 = 2.85$, $L_{m1} = 1.1$, $L_{S4} = 1.32$, $W_{S4} = 0.2$, $y_4 = 0.5$, $y_5 = 0.4$, $P_{S3} = 4.75$, all in mm.

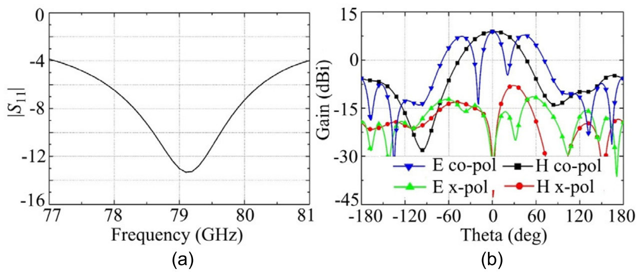

FIGURE 3. Simulated results of the TM_{05}-mode patch: (a) $|S_{11}|$ response. (b) Radiation patterns at 79 GHz.

Fig. 2 shows the configuration of the single-ended fed TM_{05}-mode patch with a resonant length of $5\lambda_g/2$. The patch is located on the upper substrate Sub 1, and an SIW feed is built into the lower substrate Sub 2 with a coupling slot in the ground plane GND 1. The numerical simulations for this design were conducted through an EM simulation tool, ANSYS HFSS.

The simulated $|S_{11}|$ response of the TM_{05}-mode patch in Fig. 2 is illustrated in Fig. 3(a), which shows a center frequency of 79 GHz and a -10-dB impedance bandwidth from 78.6 to 79.63 GHz (1.3%). Fig. 3(b) displays the simulated radiation patterns at 79 GHz with a gain of 8.8 dBi, an E-plane SLL of -1.15 dB, and a cross-polarization level of -7.9 dB. The high SLL and the unexpected low gain are attributed to the reverse currents.

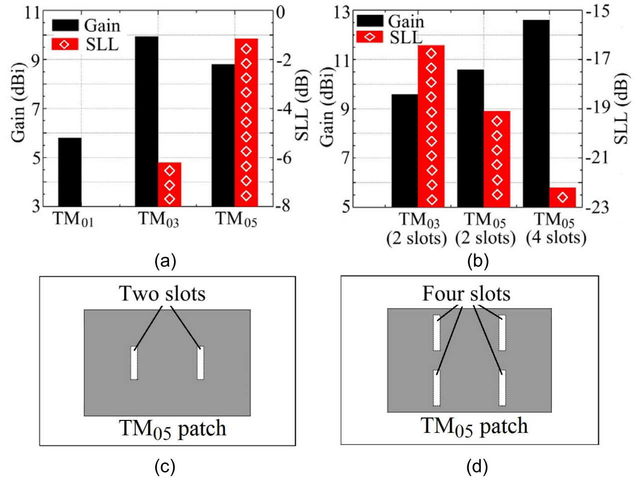

FIGURE 4. Comparison on the gain and SLL of high-order mode patches: (a) Single-ended fed patch without slots. (b) Differential-fed patch with slots. Configurations: (c) TM_{05}-mode patch with two slots. (d) TM_{05}-mode patch with four slots.

B. DIFFERENTIAL-FED FOUR-SLOT TM_{05}-MODE PATCH ANTENNA

Fig. 4(a) compares the gain and SLLs of single-ended fed TM_{01}-, TM_{03}-, and TM_{05}-mode patches without slots. The traditional TM_{01}-mode patch presents a gain of 5.8 dBi with no side lobes. The TM_{03}-mode patch exhibits increased gain due to its larger electric size, but at the expense of the high SLL. For the TM_{05}-mode patch, the reverse currents seriously deteriorate the SLL and considerably lower the gain. Introducing slots to the patch in higher-order mode is a proposed solution for the above problems. In this work, slots are placed in the TM_{05}-mode patch to suppress the reverse currents. Fig. 4(b) demonstrates that the differential-fed slotted patch in TM_{05} mode exhibits more gain and less SLL. The improved gain can be greater than 12 dBi and the SLL can be lower than -22 dB. The four-slot design in Fig. 4(d) outperforms the two-slot design in Fig. 4(c). Therefore, the TM_{05}-mode patch with four slots is selected for this work. Traditional single-ended feeding suffers from high H-plane cross-polarization, as shown in Fig. 3(b). The problem can be solved through differential feeding. Figs. 5(a) and 5(b) show the differential-fed TM_{05}-mode patch. The signals from the two slots in GND 1 exhibit the same amplitude, but a phase difference of 180°. Four symmetrical slots are created in the patch at the locations of $3L_1/10$ and $7L_1/10$, where the reverse currents are intense. The longer sides of these slots are oriented in a direction perpendicular to the direction of the resonant currents. Since the slot would change the resonant frequency of the patch, the length L_1 of the patch with these slots is slightly shorter than that of the patch without slots, while the width W_1 is slightly wider. The dimensions of the proposed patch antenna are provided in the caption of Fig. 5.

Fig. 6 shows the simulated radiation patterns subject to the changes in the slot length L_S1 at 79 GHz. The increase of the slot length L_S1 significantly decreases the E-plane SLL,

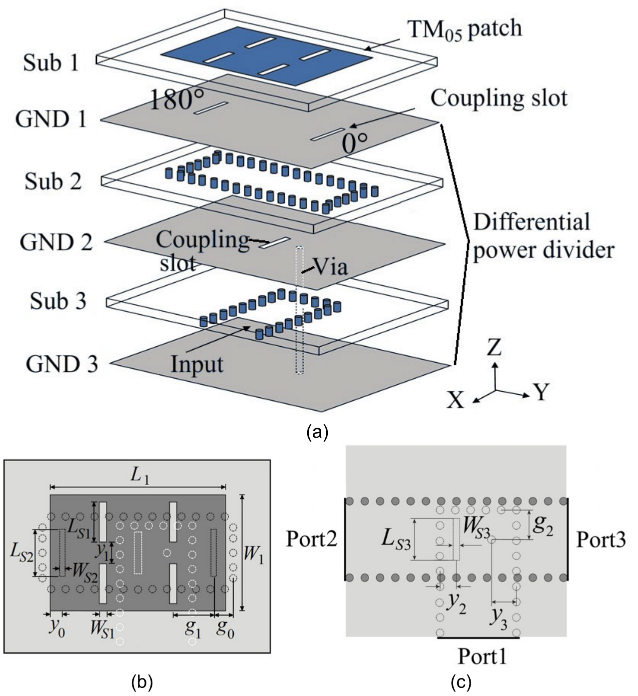

FIGURE 5. Differential-fed TM_{05}-mode patch with four slots: (a) 3D structure. (b) Geometry. (c) Differential power divider only. Each substrate is RO4003C, with $\varepsilon_r = 3.55$, $\tan\delta = 0.0027$, and a thickness of 0.305 mm. Dimensions: $L_1 = 4.9$, $W_1 = 3.2$, $L_{S1} = 1.1$, $W_{S1} = 0.2$, $L_{S2} = 1.35$, $W_{S2} = 0.15$, $y_0 = 0.36$, $g_0 = 0.55$, $y_1 = 0.6$, $g_1 = 1.47$, $L_{S3} = 1.1$, $W_{S3} = 0.17$, $y_2 = 0.43$, $y_3 = 0.65$, $g_2 = 0.77$, all in mm.

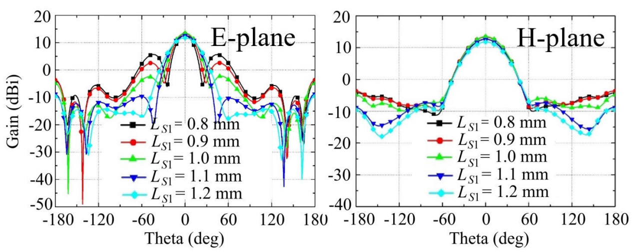

FIGURE 6. Simulated radiation patterns of the TM_{05}-mode patch subject to the changes in the slot length L_{S1} at 79 GHz.

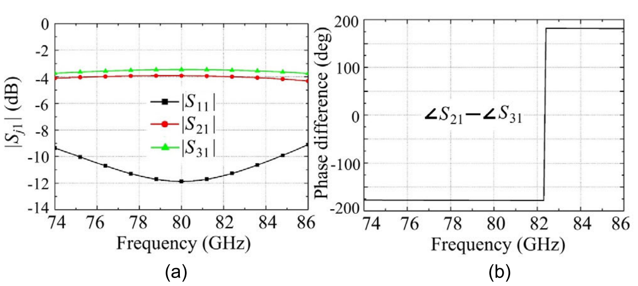

FIGURE 7. Simulated S parameters of the differential power divider: (a) Amplitude. (b) Phase difference.

confirming the use of the slots to effectively improve the radiation pattern.

An SIW differential power divider is presented alone in Fig. 5(c) for simulation analysis. The simulated S parameters is displayed in Fig. 7. The impedance bandwidth ranges from 75.14 to 84.66 GHz (12%), where the insertion loss is less than 1 dB, and the phase difference is 180±2°, presenting excellent performance. Fig. 8 shows the simulated $|S_{11}|$ response and radiation pattern of the four-slot TM_{05}-mode patch fed by the differential power divider at 79 GHz. The figure shows a gain of 12.17 dBi and an E-plane SLL lower than -24.27 dB within the impedance bandwidth from 78.96 to 79.38 GHz (0.53%). The differential feeding scheme results in a symmetrical co-polarization pattern and a cross-polarization level less than −30 dB.

C. ANALYSIS OF 1 × 2 ARRAYS ARRANGED ALONG THE E-PLANE AND H-PLANE DIRECTIONS

An array design can further increase the antenna gain. The size of the TM_{05}-mode patch is $1.29\lambda_0 \times 0.84\lambda_0$. For a linear array of the TM_{05}-mode patches extending along the E-plane (E-plane array for short), its array spacing is more than $1\lambda_0$, which would cause a grating lobe problem. According to array theory, the total radiation pattern of an array is the product of an element pattern and an array factor (AF). The grating lobe of the AF can be reduced substantially if it is located at a radiation null of the element pattern.

Fig. 9 shows a 1 × 2 E-plane array of the TM_{05}-mode patches. The element radiation pattern from Fig. 8(b) shows radiation nulls at the angle of ±45°. The array spacing required to locate the grating lobe of the AF at the null angle can be obtained via the equation below,

$$\theta_k = \cos^{-1}\left(\frac{\pm 2k\pi}{\beta d_e}\right), k = 0, 1, 2, \tag{2}$$

where k and θ_k are the number and angle of the grating lobes, respectively. k equals 0 for the main lobe, and the rest for the grating lobes. For $\theta_k = \pm 45°$, the required array spacing d_e is approximately equal to $1.41\lambda_0$.

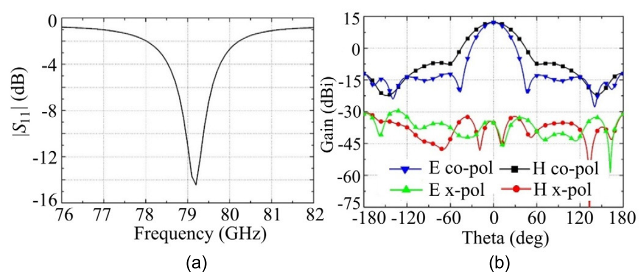

FIGURE 8. Simulated results of the differential-fed TM_{05}-mode patch with four slots: (a) $|S_{11}|$ response. (b) Radiation patterns at 79 GHz.

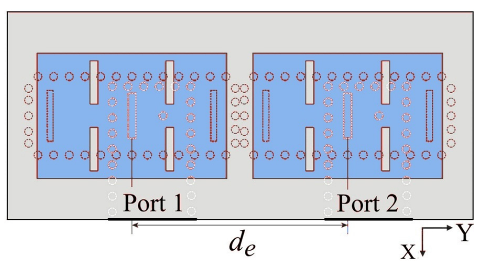

FIGURE 9. Configuration of the 1 × 2 E-plane array.

Fig. 10 shows the AF of the 1 × 2 E-plane array with $d_e = 1.41\lambda_0$. The figure demonstrates the grating lobes precisely aligned with the radiation null of the element pattern. The radiation patterns of the 1 × 2 E-plane array subject to the changes in d_e are illustrated in Fig. 11, confirming this design parameter can effectively reduce the SLL. The excessive increase of the array spacing deteriorates the SLL. Considering the SLL performance and fabrication limitations of PCB, $d_e = 1.45\lambda_0$ is selected. The mutual coupling between two elements of the 1 × 2 E-plane array can be examined through its $|S_{21}|$ response. As can be seen from Fig. 12(a), the coupling is less than −30 dB. The radiation patterns of the E-plane array at 79 GHz are provided in Fig. 12(b). The gain is 14.57 dBi, and the E-plane and H-plane SLLs are −13.15 dB and -20 dB, respectively, confirming the significant reduction of grating lobes.

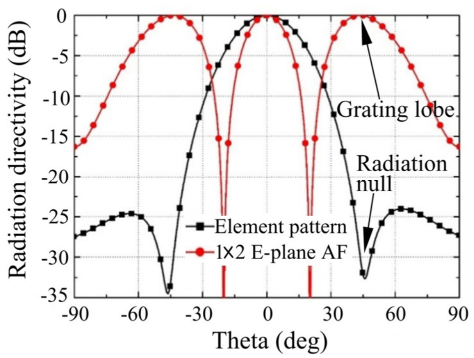

FIGURE 10. E-plane element pattern of the TM_{05}-mode patch and the AF of the 1 × 2 E-plane patch array with $d_e = 1.41\lambda_0$.

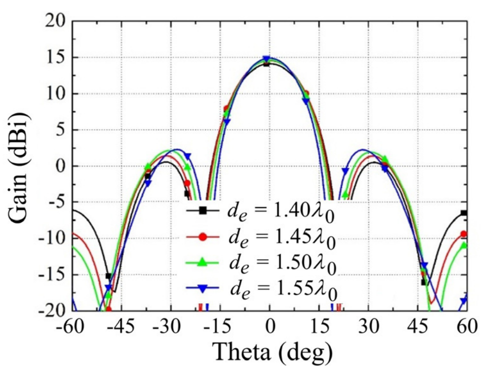

FIGURE 11. Simulated E-plane radiation patterns of the 1 × 2 E-plane array subject to the changes in the array spacing d_e.

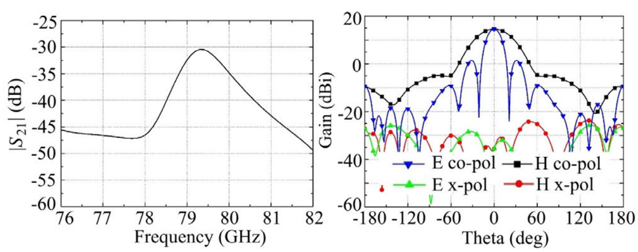

(a) (b)

FIGURE 12. Simulated results of the 1 × 2 E-plane array: (a) $|S_{21}|$ response. (b) Radiation patterns at 79 GHz.

Fig. 13 shows a 1 × 2 patch array extending along the H-plane (H-plane array for short). Since the H-plane dimension of the patch is smaller, the required array spacing is less. Fig. 14(a) shows the simulated $|S_{21}|$ responses of the H-plane array subject to the changes in the array spacing d_h. As d_h increases, the mutual coupling between the patches decreases, however, in return for the problem of grating lobes. As a compromise, $d_h = 1.1\lambda_0$ is selected for this work to ensure no grating lobe and the mutual coupling less than −25 dB. Fig. 14(b) displays the radiation patterns of the H-plane array, which indicate the antenna gain of 15 dBi and the SLLs of −21.3 dB and −16.1 dB in the E-plane and H-plane, respectively.

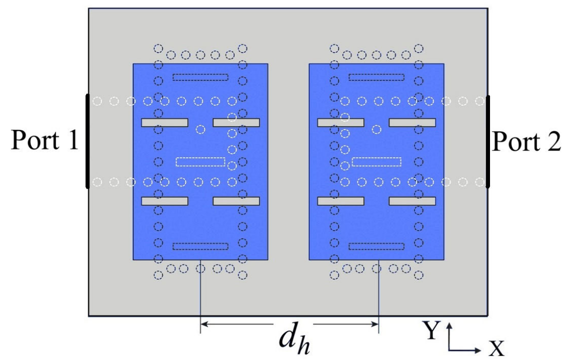

FIGURE 13. Configuration of the 1 × 2 H-plane array.

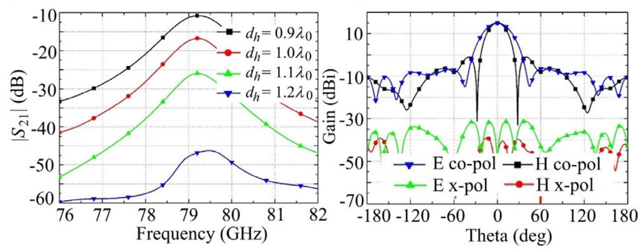

(a) (b)

FIGURE 14. Simulated results of the 1 × 2 H-plane array: (a) $|S_{21}|$ responses. (b) Radiation patterns at 79 GHz.

TABLE 1. Amplitude ratios and S parameters for the − 25-dB Eight-element taylor distribution.

Element No.	1	2	3	4	5	6	7	8
Amplitude ratio	0.393	0.592	0.843	1	1	0.843	0.592	0.393
Theoretical S parameter (dB)	-14.56	-11.03	-7.95	-6.47	-6.47	-7.95	-11.03	-14.56
Simulated S parameter (dB)	-15.99	-12.47	-9.29	-7.81	-7.81	-9.29	-12.47	-15.99
Simulated S parameter with $\tan\delta = 0$ (dB)	-14.76	-11.22	-8.03	-6.55	-6.55	-8.03	-11.22	-14.76

D. DESIGN OF −25-DB EIGHT-ELEMENT TAYLOR FEEDING NETWORK

A 2 × 8 patch array antenna with a -25-dB eight-element Taylor feeding network is presented to further reduce the H-plane SLL and to increase the gain. The amplitude ratio

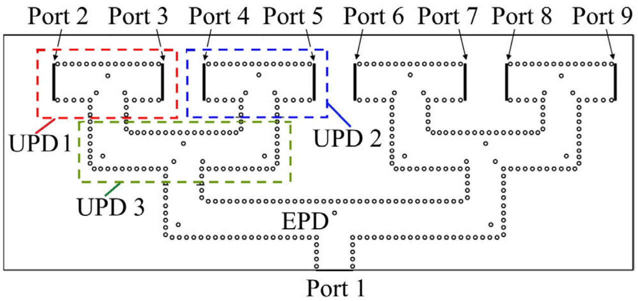

FIGURE 15. One-to-eight SIW feeding network with −25-dB Taylor distribution.

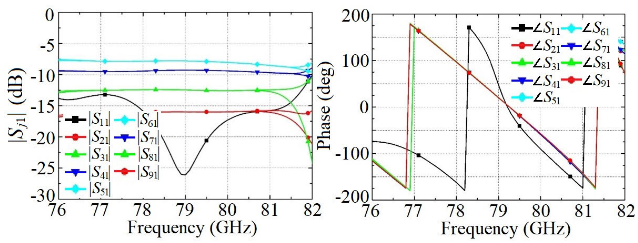

FIGURE 16. Simulated *S*-parameter responses of the one-to-eight SIW feeding network with −25-dB Taylor distribution.

of this network is 0.393:0.592:0.843:1:1:0.843:0.592:0.393, and the corresponding *S* parameters are shown in Table 1.

Fig. 15 shows a one-to-eight SIW feeding network, which is composed of an equal power divider (EPD) and three unequal power dividers (UPD1, UPD2, UPD3). The amplitude differences between the two output ports of UPD1, UPD2, and UPD3 are 3.53 dB, 1.48 dB, and 5.3 dB, respectively, which match the theoretical *S* parameters listed in Table 1 for the -25-dB Taylor distribution ratio.

Fig. 16 shows the simulated *S* parameters of the one-to-eight SIW feeding network with the -25-dB Taylor distribution ratio. A phase difference of $\pm 2^{\circ}$ is observed across the frequency range of 78 to 80 GHz. Table 1 compares the simulated and the theoretical *S* parameters of the one-to-eight feeding network. The simulated values are slightly lower than the theoretical values, but the amplitude ratios between the output ports are nearly the same. Since the dielectric loss of the substrate affects the *S* parameters, Table 1 also lists the simulated *S* parameters without the dielectric loss, which are very close to the theoretical values with an error of less than 0.2 dB.

E. FABRICATION AND MEASURED RESULTS

Fig. 17 shows the proposed 2 × 8 TM_{05}-mode patch array antenna (Antenna I) with a GCPW feed and with the H-plane array weighted by a -25-dB Taylor distribution. There are four layers of substrates in this structure with each layer supplied by RO4003C featuring a dielectric constant of 3.55 and a thickness of 0.305 mm. A two-layer one-to-four differential feeding network is placed in Sub 2 and Sub 3 to provide not only differential feeding but also power distribution for each E-plane array. A scheme of slot couplings in parallel is developed for the feeding network to generate a 32-way power distribution, which turns into 16 sets of differential input signals to excite the 16 patches.

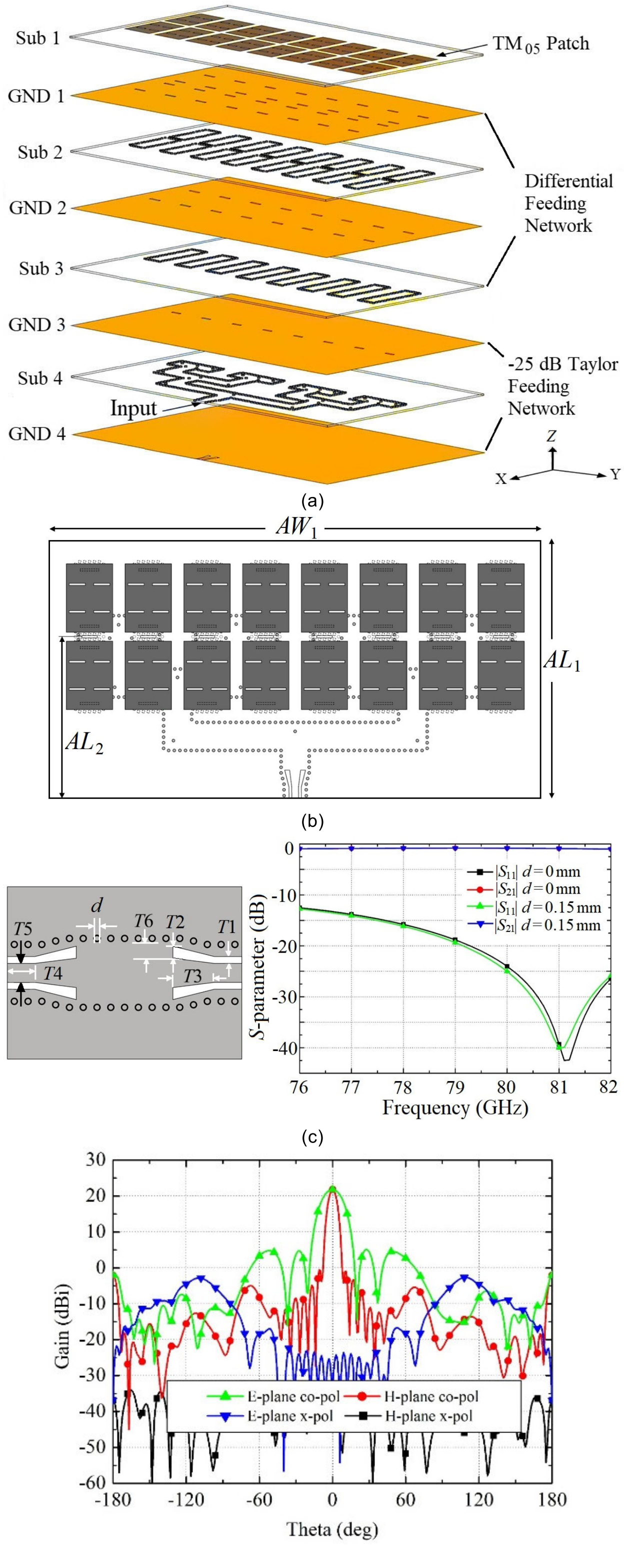

FIGURE 17. 2 × 8 patch array antenna with taylor distribution (Antenna I): (a) 3D view. (b) Top view. (c) Back-to-back GCPW-to-SIW transition and simulated *S*-parameters. (d) Simulated radiation patterns at 79 GHz. Dimensions: $AL_1 = 20.69$, $AL_2 = 14.65$, $AW_1 = 35$, $T1 = 0.2$, $T2 = 0.35$, $T3 = 1.2$, $T4 = 0.8$, $T5 = 0.48$, $T6 = 0.51$, all in mm.

To reduce manufacturing cost, this design uses hollow vias, with copper plating applied only on the via inner wall surface. To verify the performance of the GCPW-to-SIW transition, Fig. 17(c) shows the back-to-back GCPW-to-SIW transition and simulated S-parameters, where d is the inner diameter of the hollow via. At 79 GHz, the solid via achieves $|S_{11}| = -18.83$ dB and $|S_{21}| = -0.82$ dB, while the hollow via achieves $|S_{11}| = -19.36$ dB and $|S_{21}| = -0.81$ dB, demonstrating similar and good performance. The simulated results observed in Fig. 17(d) indicate the antenna gain of 21.8 dBi, the SLLs of -16.7 dB and -22.41 dB in the E-plane and H-plane, respectively, and the cross-polarization level of more than -40 dB lower than the co-polarization level near the broadside direction.

Each layer of Antenna I was manufactured separately and locked with plastic screws. For measurements, a 1.0 mm W-band end-launch connector was mounted on the edge of the structure and next to the input of the -25-dB Taylor feeding network. Fig. 18 shows the photographs of Antenna I with screw locking and a design for surface wave suppression. The use of screw locking requires a larger mounting area, which could cause surface waves to radiate through the edge of the ground plane, resulting in a concave main lobe. To solve this problem, a grounded surrounding is introduced to the patch array to suppress surface waves, as shown in Fig. 18.

Fig. 19 compares the simulated impedance bandwidth of Antenna I to the measured one, which is 78.37–79.31 GHz (1.2%) versus 77.92–79.15 GHz (1.6%). Its radiation patterns at 79 GHz are illustrated in Fig. 20. The measuring angle is only confined to $\pm 90°$ due to the limitation of measuring equipment. The simulated gain is 19.06 dBi in contrast to the measured gain of 18.2 dBi. The simulated SLLs are -12.68 dB and -24.89 dB in the E-plane and H-plane, respectively, whereas the measured SLLs in the two planes are -15.4 dB and -19.1 dB, respectively. The measured cross-polarization level is about 30 dB lower than the measured co-polarization level. Compared to the simulated performance in Fig. 17(c), the additional efforts for screw locking and surface wave suppression lead to decrease in gain and increase in SLLs. A PCB lamination can be solution for the problem. PCB lamination can provide mechanical stability without the need for external screw fixation, eliminating surface wave effects caused by screws and enlarged substrates, and maintaining electromagnetic cleanliness.

III. 77 GHz STAGGERED SERIES-FED SIX-ELEMENT TM_{05}-MODE PATCH ARRAY ANTENNA

In this section, a 77 GHz series-fed six-element TM_{05}-mode patch array antenna is proposed to achieve the goal of high gain, compact feeding network, and bandwidth enhancement. Series feed offers the advantage of small size. However, due to overlapping transmission paths, array elements can be easily interfered by one another, which increases the level of difficulty in design. A simple staggered in-phase feeding structure with an array spacing of $1.5\lambda_g$ is proposed for this work. Fig. 21 shows a 77 GHz single-ended fed

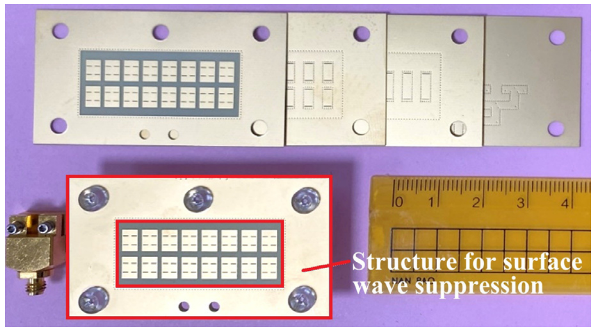

FIGURE 18. Photographs of Antenna I added with screw locking and the design for surface wave suppression.

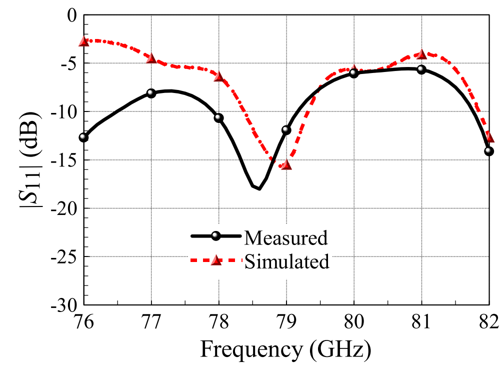

FIGURE 19. Measured and simulated $|S_{11}|$ responses of Antenna I.

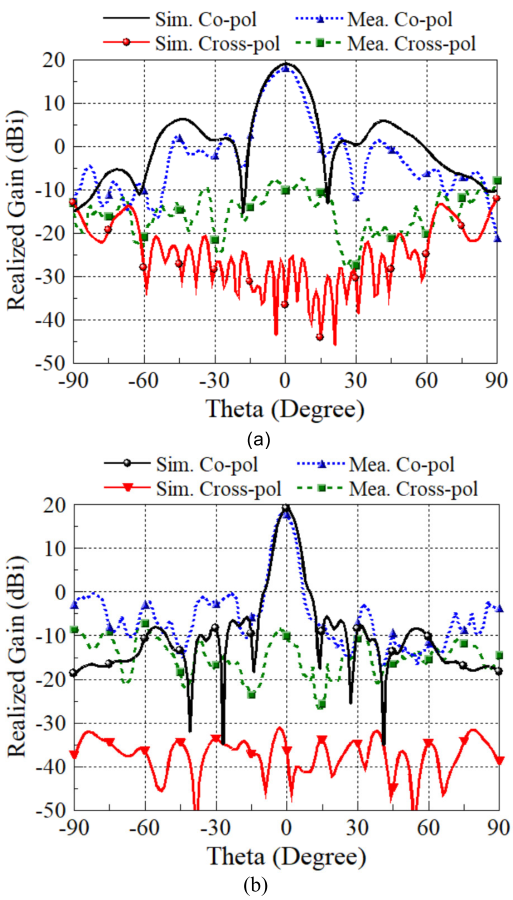

FIGURE 20. Measured and simulated radiation patterns of Antenna I at 79 GHz: (a) E-plane. (b) H-plane.

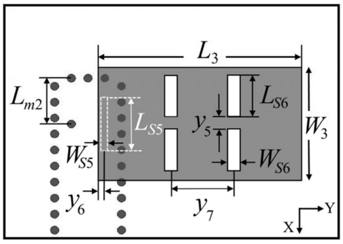

FIGURE 21. 77 GHz single-ended fed TM_{05}-mode patch antenna. Each substrate is RO4003C, with $\varepsilon_r = 3.55$, $\tan\delta = 0.0027$, and a thickness of 0.305 mm. Dimensions: $L_3 = 4.5$, $W_3 = 2.9$, $L_{s5} = 1.3$, $W_{s5} = 0.2$, $L_{s6} = 1$, $W_{s6} = 0.3$, $L_m2 = 1.1$, $y_5 = 0.45$, $y_6 = 0.2$, $y_7 = 1.5$, all in mm.

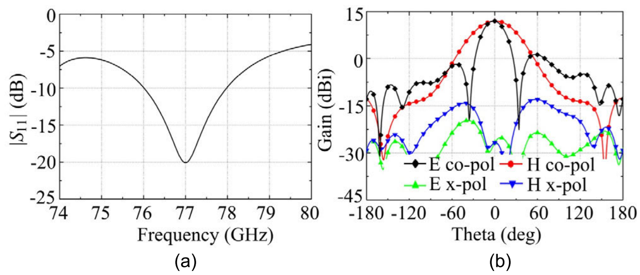

FIGURE 22. Simulation results of the TM_{05}-mode patch antenna: (a) $|S_{11}|$ response. (b) Radiation patterns at 77 GHz.

TM_{05}-mode patch. This high-order-mode patch follows the design described in Section II, however, with its dimensions adjusted to suit the operating frequency of 77 GHz. The simulation results indicate an impedance bandwidth of 76.01−77.98 GHz (2.5%), an antenna gain of 11.94 dBi, and an SLL of −10.56 dB, as shown in Fig. 22.

A. DESIGN OF STAGGERED SERIES-FED PATCH ARRAY ANTENNA

An array requires its elements to be excited in phase to achieve maximum gain. Fig. 23(a) shows a series slot-fed two-element array. The magnetic field lines inside the SIW transmission line at the locations of the two adjacent coupling slots separated by $\lambda_g/2$ are in opposite directions. Since these lines at any two locations mirrored from the SIW center line are in anti-phase, the magnetic field lines at the two sequential slots can be made in the same direction if one of the slots is moved to the other side of the center line. The direction of the patch current is perpendicular to the direction of the SIW transmission line. To achieve in-phase excitation, the locations of the patches as well as their corresponding coupling slots must be carefully chosen.

Assuming that the direction of the magnetic field lines at Patch 1 is counterclockwise, the direction of the induced current is upward. If Patch 2 is excited by a slot next to the one to excite Patch 1, as shown in Fig. 23(b), the magnetic field lines at Patch 2 would be clockwise, and the resulting patch current is downward, which is by no means in-phase excitation. A staggered design requires the sequential coupling slots on the opposites sides of the SIW center line, so the currents on the two patches are in phase. The goal of in-phase excitation can be achieved if the spacing between

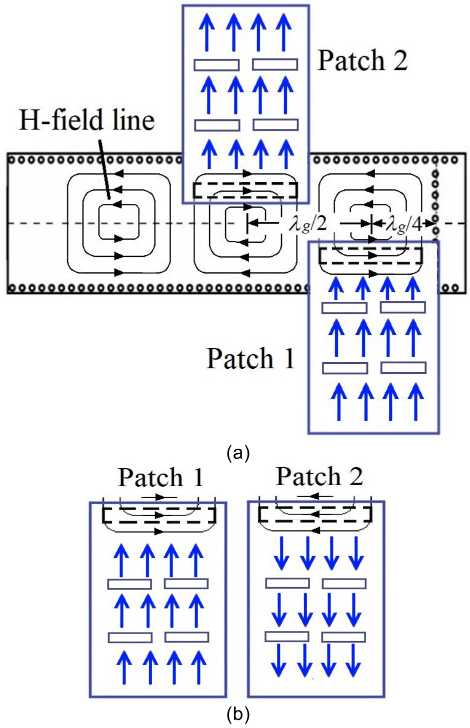

FIGURE 23. Schematic diagram: (a) SIW series-fed slot-coupled patch array. (b) Magnetic field lines and the excitation currents on the patches.

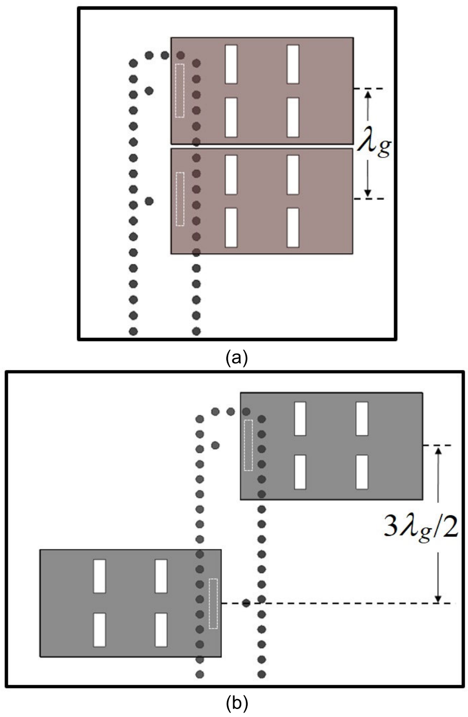

FIGURE 24. Two possible configurations of a two-element patch array: (a) Unilateral array. (b) Staggered array.

the two sequential staggered elements is an odd multiple of $\lambda_g/2$. Since the width of the TM_{05}-mode patch is larger than $\lambda_g/2$, the element spacing is chosen to be $3\lambda_g/2$ (or $1.08\lambda_0$).

Fig. 24 shows two possible configurations of a two-element patch array for in-phase excitation. The patches in Fig. 24(a)

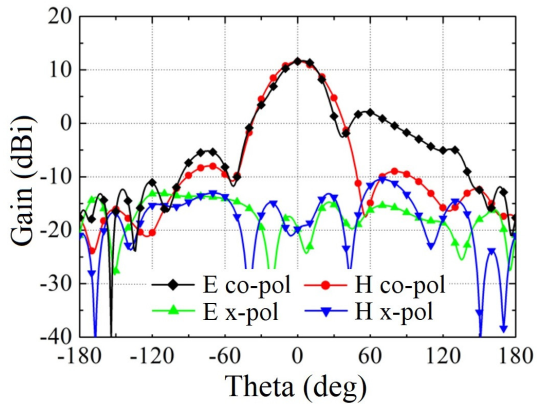

(a)

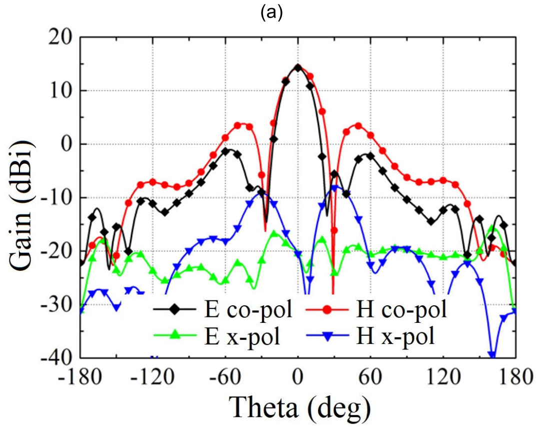

(b)

FIGURE 25. Simulated radiation patterns of the two-element TM_{05}-mode patch arrays: (a) Unilateral array. (b) Staggered array.

are aligned along the H-plane and located on the same side of the SIW with an array spacing of $1\lambda_g$ ($0.72\lambda_0$). Fig. 24(b) shows the patches in a staggered configuration along the SIW center line with an array spacing of $3\lambda_g/2$. The simulated radiation patterns of these two array configurations are demonstrated in Fig. 25. The radiation patterns of the array in Fig. 24(a) are distorted due to mutual coupling. Its gain is only 11.58 dBi, which is even lower than the gain of a single patch, 11.94 dBi. The staggered design reduces mutual coupling, which significantly increases the gain to 14.26 dBi. Although the staggered array requires larger array spacing, the consequential problem of grating lobe is not severe. As mentioned in Section II-C, the grating lobe of AF can be reduced substantially by the element pattern. This is confirmed by the results in Fig. 25(b).

B. FABRICATION AND MEASUREMENT OF THE SERIES-FED SIX-ELEMENT PATCH ARRAY ANTENNA (ANTENNA II)

Fig. 26 shows the proposed staggered series-fed six-element TM_{05}-mode patch array antenna (Antenna II). The optimized array spacing is $1.13\lambda_0$. Other design parameters are described in Fig. 26(b) with their dimensions detailed in the caption.

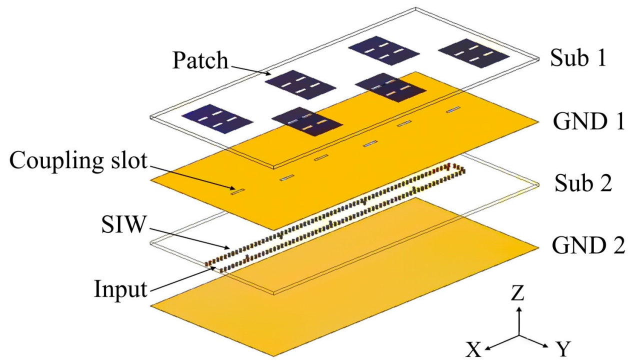

(a)

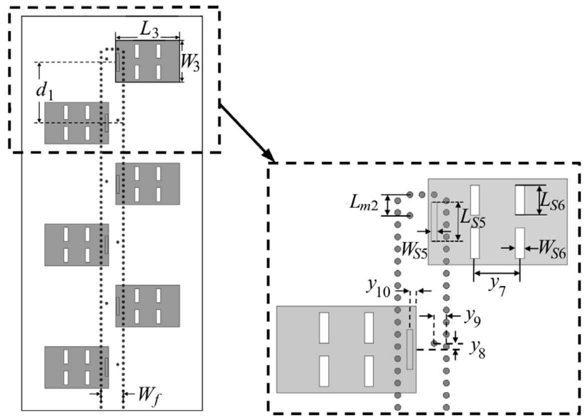

(b)

FIGURE 26. Staggered series-fed six-element TM_{05}-mode patch array antenna (Antenna II): (a) 3D view. (b) Dimensions ($L_3 = 4.6$, $W_3 = 2.9$, $W_f = 1.6$, $d_1 = 4.4$, $L_{S5} = 1.3$, $W_{S5} = 0.25$, $L_{S6} = 1$, $W_{S6} = 0.3$, $L_{m2} = 0.7$, $y_7 = 1.54$, $y_8 = 0.2$, $y_9 = 0.4$, $y_{10} = 0.15$, all in mm).

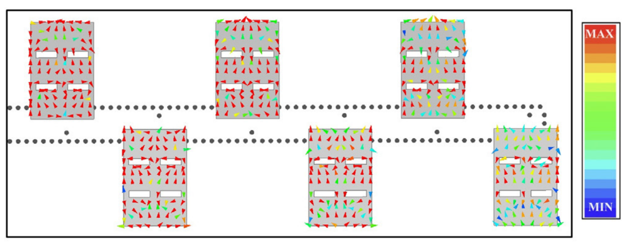

(a)

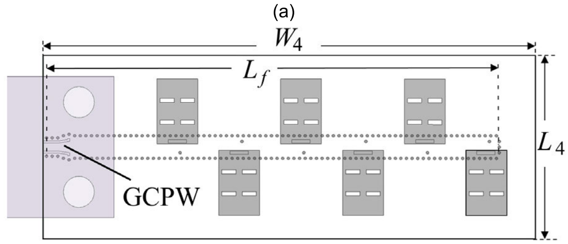

(b)

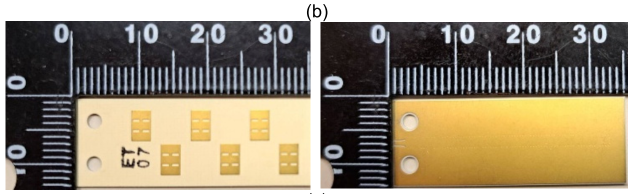

(c)

FIGURE 27. Antenna II: (a) Surface current distribution. (b) Geometry. (c)Front and back photographs. ($L_4 = 13$, $W_4 = 35$, $L_f = 32.2$, all in mm).

Fig. 27(a) shows that the simulated excitation currents on all the patches are in phase. Antenna II was fabricated

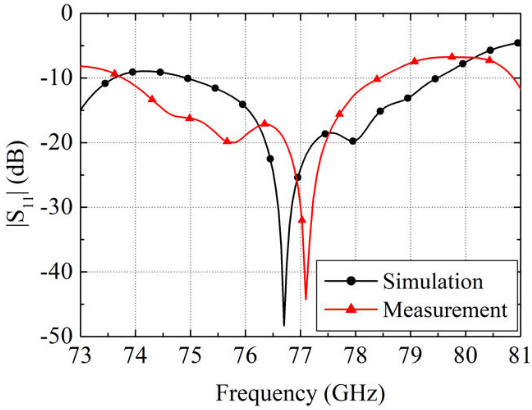

FIGURE 28. Measured and simulated $|S_{11}|$ responses of Antenna II.

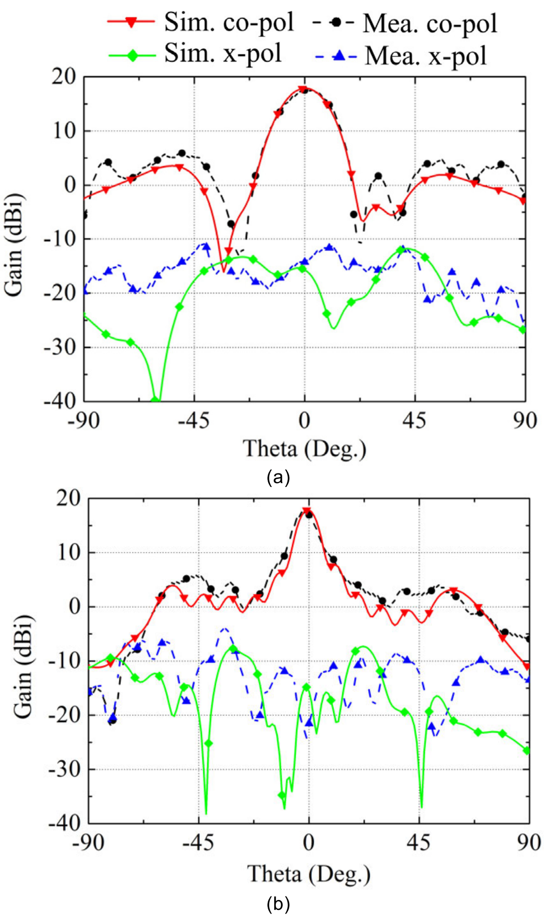

FIGURE 29. Measured and simulated radiation patterns of Antenna II at 77 GHz: (a) E-Plane and (b) H-Plane.

for experimental verification. Sub 1 was supplied by Rogers 4450F with $\varepsilon_r = 3.52$, while Sub 2 by Rogers RO4003C with $\varepsilon_r = 3.55$. Both substrates share the same thickness of 0.305 mm. A GCPW-to-SIW transition structure displayed in Fig. 27(b) is introduced to the input port for measurements. The photographs of the fabricated Antenna II are provided in Fig. 27(c).

Fig. 28 compares the simulated impedance bandwidth of 74.92–79.48 GHz (5.9%) to the measured impedance

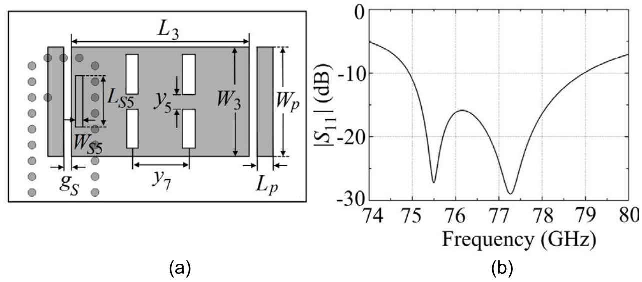

FIGURE 30. TM$_{05}$-mode patch with parasitic strips: (a) Configuration. (b) Simulated $|S_{11}|$ response. Sub 1 uses Rogers 4450F, with $\varepsilon_r = 3.52$, $\tan\delta = 0.004$, and, and a thickness of 0.305 mm; Sub 2 uses Rogers RO4003C, with $\varepsilon_r = 3.55$, $\tan\delta = 0.0027$, and a thickness of 0.305 mm. Dimensions: $L_3 = 4.5$, $W_3 = 2.77$, $L_p = 0.4$, $W_p = 2.77$, $L_{S5} = 1.3$, $W_{S5} = 0.2$, $g_S = 0.2$, $y_5 = 0.39$, $y_7 = 1.42$, all in mm.

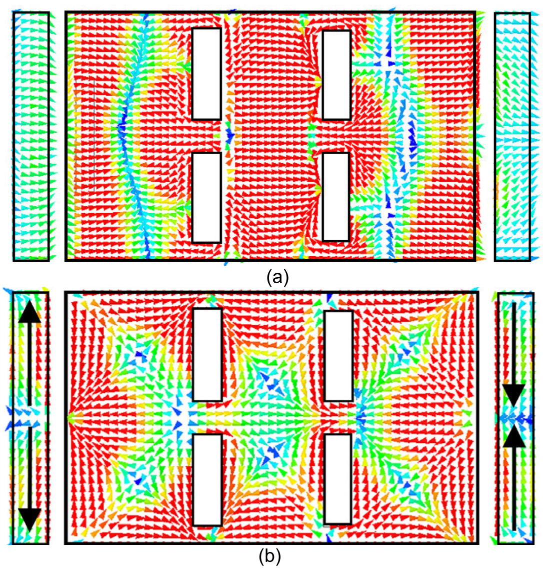

FIGURE 31. Surface current distributions of the TM$_{05}$-mode patch with the parasitic strips at: (a) 77 GHz. (b) 75.5 GHz.

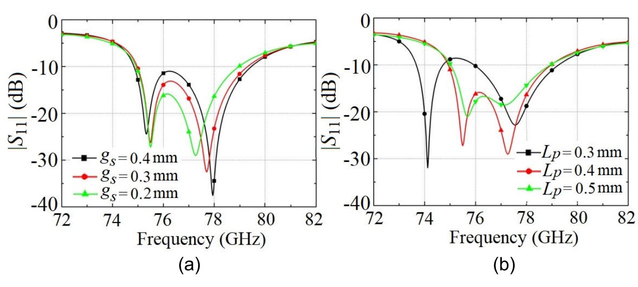

FIGURE 32. Simulated $|S_{11}|$ response of the TM$_{05}$-mode patch with parasitic strips subject to the changes in: (a) coupling spacing g_S and (b) strip width L_p.

bandwidth of 73.76–78.44 GHz (6.1%), showing only a slight shift. The simulated gain is 17.9 dBi, while the measured gain is 17.5 dBi, as indicated in Fig. 29. The simulated SLLs in the E-plane and H-plane are −14.8 dB and −10.6 dB, respectively, compared to the measured SLLs of −11.67 dB and −11.87 dB in these two planes, respectively. In general, the measured results are close to the simulated results.

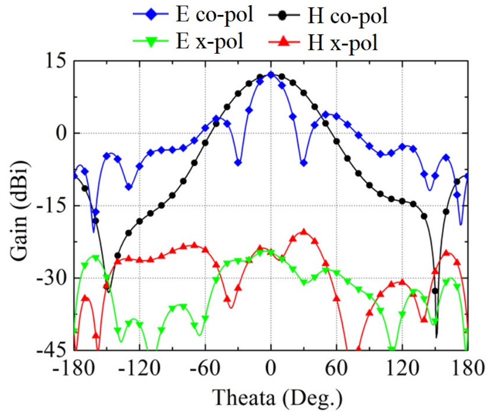

FIGURE 33. Simulated radiation patterns of the TM_{05}-mode patch with the parasitic strips at 77 GHz.

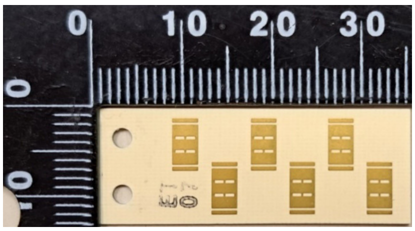

FIGURE 34. Front photograph of Antenna III with the dimensions for the optimized performance being $W_3 = 2.9$, $L_{S5} = 1.3$, $W_{S5} = 0.3$, $y_5 = 0.2$, $L_p = 0.5$, $W_p = 2.9$, $g_S = 0.4$, all in mm.

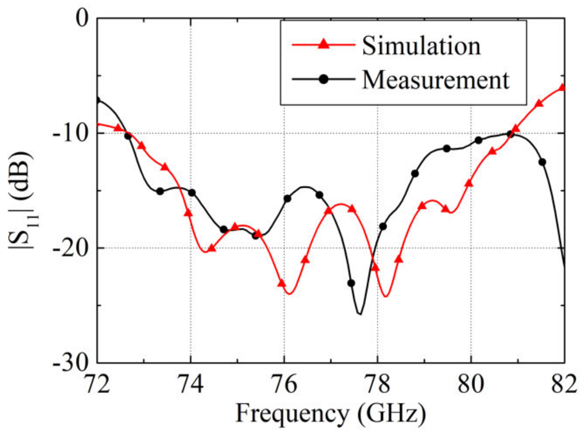

FIGURE 35. Measured and simulated $|S_{11}|$ responses of Antenna III.

C. TM_{05}-MODE PATCH WITH PARASITIC STRIPS

The bandwidth can be further increased by more than 10% to offer greater flexibility for applications. A parasitic strip is introduced next to each E-plane side of the TM_{05}-mode patch to create additional resonant poles [30−31], as shown in Fig. 30(a). The energy coupling between the main patch and each parasitic strip produces a new resonant mode. This mode corresponds to a longer equivalent electrical length and therefore resonates at a low frequency, resulting in a wider bandwidth. Compared to the $|S_{11}|$ response of the TM_{05}-mode patch without the parasitic strips, as in Fig. 22(a), a new resonant pole at 75.5 GHz appears in Fig. 30(b) in addition to the original resonance at 77 GHz.

Fig. 31(a) displays the surface current distribution at 77 GHz. The 77-GHz resonant pole is mainly contributed by the main patch, and the currents on the parasitic strips are relatively weak. The current distribution at 75.5 GHz is described in Fig. 31(b). The figure shows that the parasitic strips interact with the main patch, and their current directions are perpendicular to the current direction of the main patch. Since the directions of the currents on the upper half and the lower half of each parasitic strip are opposite, the contribution of the introduced strips to the far-field radiation pattern is trivial, but significant to the increase of the bandwidth.

Fig. 32 describes the influence of the coupling spacing g_S and strip width L_p on the $|S_{11}|$ response. As g_S increases, the two resonant poles move away from each other and the bandwidth becomes wider. Similar act can be observed by reducing L_p, but in return for the deteriorated return loss. The dimensions of the proposed design for the optimized performance are listed in the caption of Fig. 30. The optimized values for coupling spacing and strip size are g_S = 0.2 mm and L_p = 0.4 mm. These parameters are not too small and can be achieved using standard PCB manufacturing processes. The simulated impedance bandwidth presented in Fig. 30(b) ranges from 74.93 to 78.97 GHz (5.2%), which is 2.7% higher than the bandwidth of the TM_{05}-mode patch without the parasitic strips. The simulated radiation patterns at 77 GHz are displayed in Fig. 33 with a gain of 12.1 dBi, which is slightly higher than 11.94 dBi, the gain of the patch without the parasitic strips.

D. MEASUREMENT OF THE SIX-ELEMENT PATCH ARRAY WITH PARASITIC STRIPS (ANTENNA III)

The array of the TM_{05}-mode patches with the added parasitic strips is treated the same as the design from Section III-B to generate a six-element patch array, namely Antenna III. A photo of which is shown in Fig. 34. The simulated and measured impedance bandwidths of Antenna III are 72.77−80.89 GHz (10.56 %) and 72.64−80.75 GHz (10.57 %), respectively, as shown in Fig. 35. Fig. 36 shows the simulated gain of 17.9 dBi in comparison with the measured gain of 17.8 dBi. The simulated SLLs in the E-plane and H-plane are −12.3 dB and −11.6 dB, respectively, while the measured SLLs are −10 dB and −11.9 dB in these two planes, respectively. The experiment results are in good agreement with the simulated results.

Table 2 compares the performance of the proposed antennas with other published automotive antennas, in which Antenna I–III exhibit higher gain than the antennas from [5], [8], [13], [15], [19], and [20]. The H-plane SLL of Antenna I drops to −19.1 dB, which is better than the SLLs of most antennas listed in this table. In addition, Antenna I is differentially fed and thus offers the advantage of low cross-polarization. Antenna III outperforms the designs from [1], [5], [8], [13], [14], and [20] with a wider bandwidth. In summary, these proposed antennas respectively feature high gain, low SLLs, and wide bandwidth.

TABLE 2. Comparison on the performance of the proposed antennas and previously reported automotive antennas.

Ref.	Fre. (GHz)	Antenna type	Element number	BW ($\|S_{11}\|$<–10 dB)	Gain (dBi)	SLL (dB) E/H-plane	Differential Feeding	Size ($\lambda_0\times\lambda_0\times\lambda_0$)
[1]	77	Series–parallel fed patch	6×10	6.26 %	20	-15#/-12.6#	No	NP
[5]	79	Patch with dual-coupled feeding structure	2×10	4.52%#	11.8	-15.9	No	NP
[7]	24	Series-fed patch array (SFPA) & slotted EH_1-mode leaky-wave antenna	VP 12-element HP 13-element	12.9% VP# 5.8% HP#	14 VP 16.1 HP	-9 VP# -9.7 HP#	Yes	NP
[8]	79	Split-ring resonator array antenna with EBG	1×20	4.2%	12.11	-20 (H-plane)	No	13.1×0.3×0.03* 13.8×2.7×0.03**
[13]	79	Cavity-backed antenna based on SISL technology	7	6.9%	14.4	-7.8#/-11.4#	Yes	6.5×5.3×0.6
[14]	77/79	LTCC high-order mode SIW cavity with slots	8×8	6%	18.3	-15#/-11.5#	No	NP
[15]	77	Slot array with ridge gap waveguide feeding network	1×8	10.9%	14.8	-11 (*xz*-plane)	No	12.8×10.8×1.59
[19]	79	Periodic asymmetric trapezoidal perturbation microstrip antenna	1×8	11.7%	10.4	-14.4 (E-plane)	No	3.5×1.3×0.03*
[20]	77	Series-fed patch with amplitude-phase adjustment	1×8	3.6%#	14.8#	-16.6# (E-plane)	No	11.6×5.6×0.065#
[21]	79	Series-fed patch arrays with phase-adjusting power dividers	3×16 (Beam 1)	>7.6%#	18.1	-16.3# AZ -9.8# EL	No	NP
Ant. I	**79**	**2×8 TM_{05}-mode patch array with Taylor distribution**	**2×8**	**1.6%**	**18.2**	**-15.4/-19.1**	**Yes**	**9.2×5.4×0.32* 14.5×8.2×0.32****
Ant. II	**77**	**Series-fed six-element TM_{05}-mode patch array**	**6**	**6.1%**	**17.5**	**-11.67/-11.87**	**No**	**9×3.3×0.16**
Ant. III	**77**	**Six-element TM_{05}-mode patch array with parasitic strips**	**6**	**10.57%**	**17.8**	**-10/-11.9**	**No**	**9×3.3×0.16**

Fre: Frequency, BW: Bandwidth, SLL: Sidelobe level, NP: Not provided, VP: Vertically polarized, HP: Horizontally polarized,
AZ: Azimuth plane, EL: Elevation plane, #: Calculated from the graph of the referenced paper,
*: Size including only the radiating element and feeding network of the array antenna,
**: Size of the array antenna including the structure for surface wave suppression.

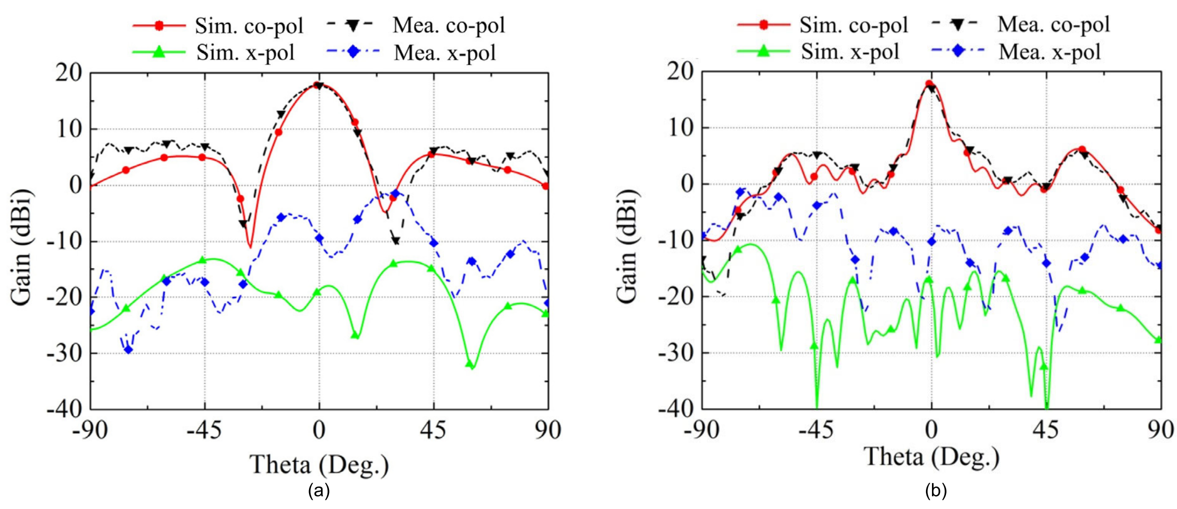

FIGURE 36. Measured and simulated radiation patterns of Antenna III at 77 GHz: (a) E-Plane and (b) H-Plane.

IV. CONCLUSION

This work presents three patch array antennas with high gain, low sidelobe, and enhanced bandwidth for automotive radar applications. The TM_{05}-mode patch is proposed with four slots in it to suppress reverse currents, which improves gain and reduces SLLs. Antenna I is a 79 GHz 2×8 array featuring a differential parallel feeding scheme and a –25-dB Taylor distribution feeding network to suppress cross-polarization and sidelobe levels. The measured data indicate an impedance bandwidth ranging from 77.92 to 79.15 GHz (1.6%), a peak gain of 18.2 dBi, and SLLs of −15.4 dB in the E-plane and −19.1 dB in the H-plane. The cross-polarization level is reduced to nearly 30 dB lower than the co-polarization level. Antenna II adopts an SIW series slot-coupled feeding network for compactness. A 77 GHz staggered series-fed six-element TM_{05}-mode patch array antenna was fabricated. The measured gain is as high as 17.5 dBi, and the measured bandwidth is 6.1%. To further increase the bandwidth, Antenna III introduces parasitic strips on the E-plane sides of each patch to generate additional resonant poles via electromagnetic coupling. This approach extends the operational bandwidth to a measured value of 10.57%, while the peak gain is not substantially disturbed with a measured value of 17.8 dBi. In summary, Antenna I achieves high gain, low SLL, and low cross-polarization with higher complexity. Antennas II/III simplify design and size while sustaining high gain and wide bandwidth. The proposed designs provide promising solutions for automotive radar antennas demanding the features of high gain, low SLL, and wide bandwidth.

REFERENCES

[1] J. Xu, W. Hong, H. Zhang, G. Wang, Y. Yu, and Z. H. Jiang, "An array antenna for both long- and medium-range 77 GHz automotive radar applications," *IEEE Trans. Antennas Propag.*, vol. 65, no. 12, pp. 7207–7216, Dec. 2017.

[2] D.-H. Shin, K.-B. Kim, J.-G. Kim, and S.-O. Park, "Design of null-filling antenna for automotive radar using the genetic algorithm," *IEEE Antennas Wireless Propag. Lett.*, vol. 13, pp. 738–741, 2014.

[3] Y. Yu, W. Hong, H. Zhang, J. Xu, and Z. H. Jiang, "Optimization and implementation of SIW slot array for both medium- and long-range 77 GHz automotive radar application," *IEEE Trans. Antennas Propag.*, vol. 66, no. 7, pp. 3769–3774, Jul. 2018.

[4] S. B. Yeap, X. Qing, and Z. N. Chen, "77-GHz dual-layer transmit-array for automotive radar applications," *IEEE Trans. Antennas Propag.*, vol. 63, no. 6, pp. 2833–2837, Jun. 2015.

[5] S. Yoo, Y. Milyakh, H. Kim, C. Hong, and H. Choo, "Patch array antenna using a dual coupled feeding structure for 79 GHz automotive radar applications," *IEEE Antennas Wireless Propag. Lett.*, vol. 19, pp. 676–979, 2020.

[6] Y. Kang, E. Noh, and K. Kim, "Design of traveling-wave series-fed microstrip array with a low sidelobe level," *IEEE Antennas Wireless Propag. Lett.*, vol. 19, pp. 1395–1399, 2020.

[7] H.-D. Li and L. Zhu, "A compact dual-polarized array antenna for automotive radar application," *IEEE Trans. Antennas Propag.*, vol. 71, no. 11, pp. 9048–9053, Nov. 2023.

[8] H. Cho, J.-H. Lee, J.-W. Yu, and B. Ahn, "Series-fed coupled split-ring resonator array antenna with wide fan-beam and low sidelobe level for millimeter-wave automotive radar," *IEEE Trans. Veh. Technol.*, vol. 72, no. 4, pp. 4805–4814, Apr. 2023.

[9] M. K. Saleem, H. Vettikaladi, M. A. S. Alkanhal, and M. Himdi, "Lens antenna for wide angle beam scanning at 79 GHz for automotive short range radar applications," *IEEE Trans. Antennas Propag.*, vol. 65, no. 4, pp. 2041–2046, Apr. 2017.

[10] W. Cao, B. Zhang, A. Liu, T. Yu, D. Guo, and Y. Wei, "Broadband high-gain periodic endfire antenna by using I-shaped resonator (ISR) structures," *IEEE Antennas Wireless Propag. Lett.*, vol. 11, pp. 1470–1973, 2012.

[11] Y. Liu, G. Bai, and M. C. E. Yagoub, "A 79GHz series fed microstrip patch antenna array with bandwidth enhancement and sidelobe suppression," in *Proc. Int. Conf. Radar, Antenna, Microw., Electron., Telecommun. (ICRAMET)*, Nov. 2020, pp. 155–158.

[12] C.-P. Chao, S.-H. Yang, C.-M. Tung, C.-F. Yang, W.-H. Lin, C.-Y. Chai, and I. Lin, "A series-fed cavity-back patch array antenna for a miniaturized 77GHz radar module," in *Proc. IEEE Int. Symp. Antennas Propag. USNC-URSI Radio Sci. Meeting*, Jul. 2019, pp. 657–658.

[13] X. Teng, Y. Luo, N. Yan, and K. Ma, "A cavity-backed antenna using SISL technology for 77 GHz band application," *IEEE Trans. Antennas Propag.*, vol. 70, no. 5, pp. 3840–3845, May 2022.

[14] Y. Shi, W. Feng, H. Wang, W. Che, Q. Xue, J. Wang, J. Zhang, X. Qian, M. Zhou, and B. Cao, "Novel W-band LTCC transition from microstrip line to ridge gap waveguide and its application in 77/79 GHz antenna array," *IEEE Trans. Antennas Propag.*, vol. 67, no. 2, pp. 915–924, Feb. 2019.

[15] Z. Zang, A. U. Zaman, and J. Yang, "Single layer dual circularly polarized antenna array based on ridge gap waveguide for 77 GHz automotive radar," *IEEE Trans. Antennas Propag.*, vol. 70, no. 7, pp. 5977–5982, Jul. 2022.

[16] W. Y. Yong, A. Haddadi, T. Emanuelsson, and A. A. Glazunov, "A bandwidth-enhanced cavity-backed slot array antenna for mmWave fixed-beam applications," *IEEE Antennas Wireless Propag. Lett.*, vol. 19, pp. 1924–1928, 2020.

[17] E. Arnieri, F. Greco, L. Boccia, and G. Amendola, "A reduced size planar grid array antenna for automotive radar sensors," *IEEE Antennas Wireless Propag. Lett.*, vol. 17, pp. 2389–2393, 2018.

[18] M. Mosalanejad, I. Ocket, C. Soens, and G. A. E. Vandenbosch, "Wideband compact comb-line antenna array for 79 GHz automotive radar applications," *IEEE Antennas Wireless Propag. Lett.*, vol. 17, pp. 1580–1583, 2018.

[19] H. Yi, Z. Wang, D. Xia, H. Liu, and L. Li, "Periodic asymmetric trapezoidal perturbation microstrip antenna for millimeter-wave automotive radar sensors," *IEEE Trans. Antennas Propag.*, vol. 71, no. 2, pp. 1369–1377, Feb. 2023.

[20] P. Zhao, N. Li, F. Wang, Y. Zhang, and N. Hu, "Beam squint suppression of series-feed microstrip patch antenna for automotive radar," *IEEE Trans. Antennas Propag.*, vol. 73, no. 5, pp. 3340–3345, May 2025.

[21] J.-H. Lee, J. M. Lee, and D.-W. Seo, "Design and evaluation of a sector beam antenna for 79-GHz short-range radar sensors," *IEEE Access*, vol. 13, pp. 39087–39095, 2025.

[22] P. Juyal and L. Shafai, "Sidelobe reduction of TM_{12} mode of circular patch via nonresonant narrow slot," *IEEE Trans. Antennas Propag.*, vol. 64, no. 8, pp. 3361–3369, Aug. 2016.

[23] D. Wang, K. B. Ng, C. H. Chan, and H. Wong, "A novel wideband differentially-fed higher-order mode millimeter-wave patch antenna," *IEEE Trans. Antennas Propag.*, vol. 63, no. 2, pp. 466–473, Feb. 2015.

[24] X. Zhang, K.-D. Hong, L. Zhu, X.-K. Bi, and T. Yuan, "Wideband differentially fed patch antennas under dual high-order modes for stable high gain," *IEEE Trans. Antennas Propag.*, vol. 69, no. 1, pp. 508–513, Jan. 2021.

[25] X. Zhang, L. Zhu, and Q.-S. Wu, "Sidelobe-reduced and gain-enhanced square patch antennas with adjustable beamwidth under TM_{03} mode operation," *IEEE Trans. Antennas Propag.*, vol. 66, no. 4, pp. 1704–1713, Apr. 2018.

[26] Y. Zhang, W. Cao, Z. Qian, S. Shi, and W. Peng, "Low grating lobe array antenna with electrically large property based on TM_{50} mode," *IEEE Access*, vol. 7, pp. 32897–32906, 2019.

[27] W. Ma, W. Cao, R. Hong, J. Jin, and B. Zhang, "Planar broadband higher-order mode millimeter-wave microstrip patch antenna array with low sidelobe level," *IEEE Antennas Wireless Propag. Lett.*, vol. 20, no. 12, pp. 2225–2229, Dec. 2021.

[28] J. Anguera, A. Andújar, and J. Jayasinghe, "High-directivity microstrip patch antennas based on TM_{odd-0} modes," *IEEE Antennas Wireless Propag. Lett.*, vol. 19, pp. 39–43, 2020.

[29] C. A. Balanis, *Antenna Theory: Analysis and Design*, 4th ed., Hoboken, NJ, USA: Wiley, 2016.

[30] H. H. Tran and N. Nguyen-Trong, "Performance enhancement of MIMO patch antenna using parasitic elements," *IEEE Access*, vol. 9, pp. 30011–30016, 2021.

[31] L. Wang, Z. Zhu, and Y. En, "Performance enhancement of broadband circularly polarized slot–microstrip antenna using parasitic elements," *IEEE Antennas Wireless Propag. Lett.*, vol. 20, pp. 2255–2259, 2021.

TING-WEI KUO was born in Taipei, Taiwan. He received the M.S. degree in electronics engineering from Chang Gung University, Taoyuan, Taiwan, in 2021. His research interest includes the design of automotive radar antennas.

YU-LIANG ZHU CHEN was born in Taoyuan, Taiwan. He received the M.S. degree in electronics engineering from Chang Gung University, Taoyuan, Taiwan, in 2023. His research interests include the design of automotive radar and 5G wireless communication antennas.

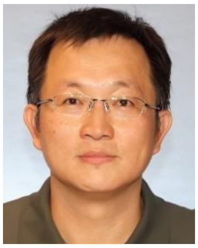

ERIC S. LI received the B.S. degree from Tamkang University, New Taipei City, Taiwan, in 1986, the M.S. degree in electrical engineering from the State University of New York, Stony Brook, NY, USA, in 1987, and the Ph.D. degree in electrical engineering from the University of Michigan, Ann Arbor, MI, USA, in 1998.

From 1988 to 1992 and from 1998 to 1999, he was a Microwave Engineer with Wireless Industries, participating in the design of microwave circuits and antennas. From 1999 to 2006, he was a Faculty Member with the Department of Electrical Engineering, National Chi Nan University, Taiwan. Since 2006, he has been with the Department of Electronic Engineering, National Taipei University of Technology, Taiwan, where he is currently a Professor. His research interests include high-frequency circuits, high-frequency calibration and measurement techniques, microwave and millimeter-wave polarimetric radar systems, and electromagnetic scattering.

HUAYAN JIN (Member, IEEE) was born in Hangzhou, Zhejiang, China, in 1989. She received the B.S. degree and the Ph.D. degree from Nanjing University of Science and Technology (NUST), Nanjing, China, in 2011 and 2017, respectively. From August 2012 to January 2013, May 2013 to October 2013, and April 2014 to October 2014, she was an Exchange Student with Chang Gung University, Taoyuan, Taiwan.

Since May 2017, she has been with Hangzhou Dianzi University, where she is currently an Associate Professor. Her main research interests include microwave and millimeter-wave antennas, differential-fed antennas, and filtering antennas.

DONGXU CHEN was born in Xuzhou, Jiangsu, China, in 1994. She received the B.Eng. and Ph.D. degrees in electromagnetic field and microwave technology from Nanjing University of Science and Technology, Nanjing, China, in 2015 and 2021, respectively. She was an Exchange Student with the Department of Electronics Engineering, Chang Gung University, from May 2017 to November 2017, and the Key Laboratory of Millimeter Waves and Terahertz, School of Electronic and Information Engineering, South China University of Technology, Guangzhou, China, from July 2018 to June 2021. Since July 2021, she has been a Lecturer with the Computer and Information College, Hohai University, Nanjing. Her main research interests include novel artificial material-based antenna arrays, metasurface antennas, millimeter-wave antenna arrays, and multi-functional antennas. She was the recipient of the Best Paper Prize of the 2015 IEEE Asia Pacific Microwave Conference, in December 2015, the Merit Paper Prize of the 2016 International Symposium on InfoComm & Media Technology in Bio-Medical & Healthcare Application, Singapore, in October 2016, and the Honorable Mention Award of the 2019 IEEE MTT-S International Wireless Symposium.

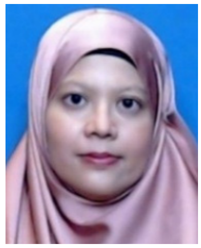

NORUN FARIHAH ABDUL MALEK (Senior Member, IEEE) received the bachelor's degree (Hons.) in communication engineering from International Islamic University Malaysia (IIUM), Kuala Lumpur, Malaysia, in 2006, and the master's degree in digital communication systems and Ph.D. degree in communication engineering from Loughborough University, in 2007 and 2013, respectively. Later, she was appointed as an Assistant Lecturer with IIUM. She was an Assistant Professor with IIUM, where she is currently an Associate Professor. She did her attachment with Intel Malaysia Sdn. Bhd. under MOHE-Intel Elite Internship Program 2020. She has secured many grants with a total amount of up to MYR500K. Her research interests include antenna and propagation, signal processing, particularly antenna arrays, algorithms, and wireless communication systems. She has been awarded the IEEE Volunteer Award 2021 by the IEEE AP/MTT/EMC Malaysia Joint Chapter Society.

KUO-SHENG CHIN (Senior Member, IEEE) received the B.S. degree in electrical engineering from the Chung Cheng Institute of Technology, Taoyuan, Taiwan, in 1986, the M.S.E.E. degree from Syracuse University, Syracuse, NY, USA, in 1993, and the Ph.D. degree in communication engineering from National Chiao Tung University, Hsinchu, Taiwan, in 2005.

From 1986 to 2005, he was with the Chung Shan Institute of Science and Technology, Taoyuan, as a Research Assistant, becoming an Assistant Scientist, and then an Associate Scientist. He joined Chang Gung University, Taoyuan, as a Faculty Member, in 2006, where he is currently a Professor with the Department of Electronic Engineering. He supervised a student team to win first place in the 2009 National Electromagnetism Application Innovation Competition, Taiwan. His current research interests include microwave and millimeter-wave couplers, filters, duplexers, low-temperature cofired ceramic circuits, automotive radar antennas, frequency-selective surfaces, filtering antennas, radomes, and electromagnetic pulse research. He was one of the recipients of the Best Paper Award of the International Conference on Electromagnetic Near Field Characterization and Imaging in 2009, the Honorable Paper Award of the International High Speed Intelligent Communication Forum in 2010, the Best Student Paper Award of the International Symposium on Next-Generation Electronics in 2014, the Best Paper Award of the Taiwan Precision Engineering Workshop in 2016, and the Best Student Paper Award of 2018 the 8th International Symposium on InfoComm and Mechatronics Technology in Bio-Medical and Healthcare Application. He also received the Outstanding Teacher Award from Chang Gung University in 2014 and 2021. He served as an Associate Editor for *Microwave and Optical Technology Letters* from 2019 to 2020.